



Published in final edited form as:

Ultrasound Med Biol. 2010 June ; 36(6): 935–948. doi:10.1016/j.ultrasmedbio.2010.03.015.

Effect of Microbubble Size on Fundamental Mode High Frequency Ultrasound Imaging in Mice

Shashank Sirsi¹, Jameel Feshitan¹, James Kwan¹, Shunichi Homma², and Mark Borden^{1,*}

¹Department of Chemical Engineering, Columbia University, New York, NY USA

²Division of Cardiology, Columbia University Medical Center, New York, NY USA

Abstract

High-frequency ultrasound imaging using microbubble (MB) contrast agents is becoming increasingly popular in pre-clinical and small animal studies of anatomy, flow and vascular expression of molecular epitopes. Currently, *in vivo* imaging studies rely on highly polydisperse microbubble suspensions, which may provide a complex and varied acoustic response. In order to study the effect of individual microbubble size populations, microbubbles of 1-2 μm , 4-5 μm , and 6-8 μm diameter were isolated using the technique of differential centrifugation. Size-selected microbubbles were imaged in the mouse kidney over a range of concentrations using a Visualsonics Vevo 770 ultrasound imaging system with a 40-MHz probe in fundamental mode. Results demonstrate that contrast enhancement and circulation persistence are strongly dependent on microbubble size and concentration. Large microbubbles (4-5 and 6-8 μm) strongly enhanced the ultrasound image with positive contrast, while 1-2 μm microbubbles showed little enhancement. For example, the total integrated contrast enhancement, measured by the area under the time-intensity curve (AUC), increased 16-fold for 6-8 μm diameter microbubbles at 5×10^7 MB/bolus compared to 4-5 μm microbubbles at the same concentration. Interestingly, 1-2 μm diameter microbubbles, at any concentration, did not measurably enhance the integrated ultrasound signal at tissue depth, but did noticeably attenuate the signal, indicating that they had a low scattering-to-attenuation ratio. When concentration matched, larger microbubbles were more persistent in circulation. However, when volume matched, all microbubble sizes had a similar circulation half-life. These results indicated that dissolution of the gas core plays a larger role in contrast elimination than filtering by the lungs and spleen. The results of this study show that microbubbles can be tailored for optimal contrast enhancement in fundamental mode imaging.

Keywords

Contrast agent; Diameter; Circulation persistence; Scattering cross-section; Absorption; Kidney

© 2010 World Federation for Ultrasound in Medicine and Biology. Published by Elsevier Inc. All rights reserved.

*Corresponding Author Address: Mark Borden, Department of Chemical Engineering, Columbia University, 500 W 120 ST, New York, NY 10027, Phone: 212-854-6955, Fax: 212-854-3044, mb2910@columbia.edu.

Publisher's Disclaimer: This is a PDF file of an unedited manuscript that has been accepted for publication. As a service to our customers we are providing this early version of the manuscript. The manuscript will undergo copyediting, typesetting, and review of the resulting proof before it is published in its final citable form. Please note that during the production process errors may be discovered which could affect the content, and all legal disclaimers that apply to the journal pertain.

Introduction

Clinical ultrasound imaging is a popular and cost-effective method of diagnosing numerous diseases. Most clinical scanners use ultrasound frequencies between 1-10 MHz. However, high-frequency ultrasound (HFU) scanners, which operate between 30 and 80 MHz, are becoming increasingly popular for small animal imaging and preclinical drug testing (Foster et al. 2000b; Coatney 2001; Foster et al. 2002; Foster et al. 2009). The use of high frequencies offers higher spatial and temporal resolution at the expense of lower signal depth penetration into the tissue, which is ideal for imaging mice and other small animals. As with clinical ultrasound scanners, circulating microbubble contrast agents increase the acoustic backscatter of HFU, making them useful for contrast enhancement of vascular anatomy, blood flow and molecular imaging (Foster et al. 2000a; Dayton and Ferrara 2002; Klibanov 2006; Klibanov 2007; Jugold et al. 2008; Palmowski et al. 2008; Migaletto et al. 2009). HFU studies in mice typically use commercially available microbubble contrast agents, such as Definity (Lantheus Medical Imaging, USA), Optison (GE Healthcare, United Kingdom) or Micro-Marker (Bracco, Italy), which are highly polydisperse in size. Definity, for example, contains a range of microbubbles from less than 1 μm to 10 μm diameter, with most of the microbubbles below 2 μm diameter (Goertz et al. 2007; Stapleton et al. 2009). Similarly, Optison contains a range of microbubble sizes between 1 and 20 μm , with 93% smaller than 10 μm (Kamaev et al. 2004). The high polydispersity is a consequence of the emulsification methods used to generate microbubbles in high quantity, such as sonication, shaking and milling. Feshitan et al. (Feshitan et al. 2009) found that lipid-coated microbubbles formed by sonication were multi-modal in size, with most bubbles between 1-2 μm and distinct subpopulations at 4-5 μm and 6-8 μm in diameter. The relative contribution of each size class to the acoustic response and circulation persistence is unclear, particularly at high frequencies. Thus, the goal of this study was to determine the role of microbubble size on intensity and duration of enhancement.

The acoustic response of small (< 2 μm) lipid-coated microbubble populations has been studied by Goertz et al. (Goertz et al. 2007). Microbubble populations were isolated using flotation or filtering to remove larger microbubbles (>1-2 μm diameter), and the acoustic attenuation (extinction) from 2 to 50 MHz was measured. Smaller microbubbles were found to attenuate more strongly at higher frequencies because they were closer to resonance, as predicted by a Rayleigh-Plesset model. The focus of that study, however, was on the non-linear response of small microbubbles. The backscattered intensity measurements of microbubbles larger than 2 μm diameter were not reported. In this study, we examined the effect of microbubble size on *in vivo* HFU fundamental-mode imaging.

The persistence time of microbubbles in circulation is another property that has important effects on contrast enhancement, molecular imaging and therapeutic strategies. The duration of the ultrasound contrast signal depends on the rate of microbubble removal from circulation due to dissolution of the gas core, filtering by the lungs and spleen, and uptake by macrophages (Ferrara et al. 2009). It is unclear which microbubble elimination mechanism dominates in contrast decay.

It is commonly believed that smaller microbubbles are able to more efficiently traverse pulmonary capillary beds, whereas larger bubbles are trapped and may even occlude flow. For example, Bouakaz et al. (Bouakaz et al. 1998b) suggested that protein-shelled Albunex microbubbles larger than the mean capillary diameter are filtered out by the lung capillary bed, thus changing the size distribution profile of circulating microbubbles. The interior pulmonary capillaries of rats range in size between 4 and 9 μm diameter, with a mean of 5 μm diameter (Short et al. 1996). Size-dependent filtering also occurs in the red pulp meshwork of the spleen, where the slit size ranges between 0.2-0.5 μm (Moghimi 1995). Tartis et al. (Tartis et al. 2008) used positron emission tomography (PET) to show that a large percentage of injected

microbubble shell material accumulates in the spleen, presumably through size-dependent filtration mechanisms. Willman et al. (Willmann et al. 2008) also used PET to show that targeted microbubble shells are taken up by the spleen.

Clearance of microbubbles from the bloodstream can also be attributed to physical removal by macrophages associated with the reticular endothelial system (RES) (Kabalnov et al. 1998). Research by Lindner et al. (Lindner et al. 2000a; Lindner et al. 2000b) suggested that lipid-based microbubbles are rapidly phagocytosed by activated neutrophils and monocytes. Willman et al. (Willmann et al. 2008) demonstrated uptake of targeted microbubbles by hepatic Kupffer cells and splenic macrophages. Because phagocytic uptake depends on surface opsonization (Moghimi et al. 2001), and filtration mechanisms may also facilitate phagocytic uptake, we hypothesized that larger microbubbles, particularly those above 5 μm diameter, would be cleared more rapidly from circulation than their smaller counterparts.

Alternatively, microbubble persistence may be governed by dissolution of the gas core. A study by Kabalnov et al. (Kabalnov et al. 1998) suggested that the primary mechanism of microbubble clearance is due to dissolution, which is brought about by the Laplace overpressure, blood pressure, and under-saturation of the filling gas. This conclusion stemmed from observations that the decay time of the ultrasound signal showed little variability between animals, only moderately increased with the administered dose, and were strongly dependent on the nature of the filling gas. More recent work by Borden et al. (Borden and Longo 2004) suggests that the observations made by Kabalnov et al. can be explained by the high permeation resistance of the microbubble shell. If dissolution is the dominant elimination mechanism of ultrasound contrast, then larger microbubbles are expected to circulate longer (Epstein and Plesset 1950; Borden and Longo 2002; Sarkar et al. 2009).

We recently developed a facile centrifugation method for isolating large quantities of size-selected microbubbles from a polydisperse suspension (Feshitan et al. 2009). Here, microbubbles are separated by size based on their relative buoyancy in a centrifugal field. By altering the centrifugal force, viscosity, time and path-length, individual size populations can easily be separated and collected. This method was shown to effectively isolate mono-modal microbubbles of 1-2 and 4-5 μm diameter at high concentrations, suitable for multiple animal injections (Feshitan et al. 2009). In the current study, we extend this technique to include isolation of 6-8 μm diameter microbubbles. We then examine contrast properties of the size-selected microbubbles in mice imaged with a commercially available HFU scanner. The results are relevant to contrast-enhanced small-animal imaging and therapeutic ultrasound.

Materials and Methods

Materials

0.01 M NaCl phosphate buffered saline (PBS) solution was prepared by dissolving salt tablets (Sigma-Aldrich) in purified water (10 M Ω -cm; Millipore) and adjusting pH to 7.4. PBS was filtered through 0.2- μm pore size polycarbonate filters (VWR, West Chester, PA). Perfluorobutane (PFB) was obtained from FluoroMed (Round Rock, TX) at >99 wt% purity. 1,2-distearoyl-*sn*-glycero-3-phosphocholine (DSPC) was purchased from Avanti Polar Lipids (Alabaster, AL) and Polyoxyethylene-40 stearate (PEG40S) was obtained from Sigma-Aldrich (St. Louis, MO).

Microbubble generation

Microbubbles were prepared as described by Feshitan et al. (Feshitan et al. 2009). Briefly, microbubbles were prepared by sonicating a lipid suspension (DSPC:PEG40S = 9:1 molar ratio) in the presence of PFB gas. The microbubble suspension was collected in 60-mL syringes

and concentrated into a cake by centrifuging the suspension at 300 relative centrifugal force (RCF) for 5 minutes using a bucket-rotor centrifuge (Model 5804, Eppendorf, Westbury, NY). The microbubble cake was saved, and infranatant was discarded. Size populations of 1-2 and 4-5 μm diameter were isolated from the microbubble suspension using the methods described by Feshitan et al. (Feshitan et al. 2009). A brief description of the size isolation protocol is presented here. All microbubbles were stored at 4 °C. Although the size-selected microbubbles are stable upon storage for at least two weeks (Feshitan et al. 2009), we used them on the same day that they were made for experimental consistency.

Size isolation of 1-2 μm bubbles

The initial microbubble sample was collected in 60 mL syringes. Microbubbles greater than 6 μm were removed by centrifuging the initial microbubble suspension at 50 RCF for 1 minute. The infranatant containing smaller bubbles was re-suspended to 60 mL with PBS, while the cake containing larger bubbles was discarded. Microbubbles greater than 3 μm diameter were removed by centrifuging the collected infranatant at 290 RCF for 1 min. The infranatant was re-suspended to 60 mL with PBS, while the cake was discarded. The collected infranatant was concentrated down to 1 mL using 300 RCF for 5 min. The sample was stored in 2-mL serum vials. The final gas concentration of the suspension was at least 1 vol% to ensure stability (Feshitan et al. 2009).

Size isolation of 4-5 μm bubbles

Microbubbles less than 4 μm diameter were removed by centrifuging at 120 RCF for 1 min. The cake was collected and reconstituted with PBS, while the infranatant was discarded. This washing step was repeated 5 to 7 times to fully remove smaller bubbles from the sample. Microbubbles greater than 6 μm were removed by centrifuging the resulting suspension at 80 RCF for 1 minute. The infranatant containing 4-5 μm microbubbles was collected, while the cake was discarded. The cake was re-suspended and centrifuged at 80 RCF for 1 minute again to completely remove the larger bubbles. The size-isolation procedure was repeated 2-3 times to collect a sufficient number of microbubbles. The resulting cakes containing 4-5 μm bubbles were combined and concentrated to 1 mL. The final gas concentration of the 4-5 μm microbubble suspension ranged from 2-5 vol%.

Size isolation of 6-8 μm bubbles

Microbubbles less than 6 μm diameter were removed by centrifuging at 60 RCF for 1 min. The cake was collected and reconstituted with PBS, while the infranatant was discarded. This washing step was repeated 5 to 7 times to fully remove smaller bubbles from the sample. Microbubbles greater than 8 μm in diameter were removed by centrifuging the resulting suspension at 40 RCF for 1 minute. The infranatant containing 6-8 μm microbubbles was collected, while the cake was discarded. The cake was re-suspended and centrifuged at 40 RCF for 1 minute to completely remove the larger bubbles. The size-isolation procedure was repeated 2-3 times to produce enough 6-8 μm bubbles for storage. The resulting cakes containing 6-8 μm bubbles were combined and concentrated to 1 mL. The final gas concentration of the 6-8 μm microbubble suspension ranged from 2-10 vol%.

Polydisperse microbubbles

Polydisperse lipid-coated microbubbles characterized in this study were produced by the shaking method, which was developed for the commercially available ultrasound contrast agent, Definity (Unger 1992). In this procedure, 2 mL of the lipid solution in sterile-filtered PBS (2 mg/mL) was warmed to 60 °C in a sealed 3-mL glass serum vial (Wheaton, Millville, NJ) and briefly bath sonicated to disperse the lipid. The air headspace was exchanged with PFB by attaching the serum vial containing the lipid solution to a 3-way valve connected to

both the gas canister and vacuum line. The lipid solution was maintained under vacuum to remove the air. The position of the valve was switched to close the vacuum line and immediately flood the headspace with PFB gas. This procedure was repeated five times to ensure complete gas exchange. The pressure in the vial was vented briefly to the atmosphere, and the microbubbles were formed by rapidly shaking the vial for 45 seconds using a VialMix (Bristol-Myers Squibb). The resulting microbubble suspension was used without further processing.

Particle Counting and Size Analysis

Microbubble size distributions and concentrations were determined by laser light obscuration and scattering (Accusizer 780A, NICOMP Particle Sizing Systems, Santa Barbara, CA). 2- μL samples of each microbubble suspension were diluted into a 30-mL flask under mild mixing during measurement. Concentrations and size distributions of each sample were measured before injection in triplicate. Previous optical microscopy results have shown that the Accusizer is accurate in measuring size distributions (Feshitan et al. 2009). The Accusizer laser provides uniform illumination across the sample path. Size analysis was confirmed using a Coulter Multisizer III (Beckman Coulter, Opa Locka, FL). A 5- μL sample of microbubble suspension was diluted into a 60-mL flask and stirred continuously to prevent flotation-induced error. A 30- μm aperture (size range of 0.6-18 μm) was used for the measurements.

Animal Injections

All animal experiments were approved by the Columbia University Institutional Animal Care and Use Committee. Contrast persistence studies were performed in female CD-1 mice 4-6 weeks of age (Charles River Laboratories, Wilmington, MA). Mice were anesthetized using 1-2% isoflurane and placed on a mouse handling table, and the heart rate, respiratory rate, and temperature were monitored using a TMH-150 physiological monitoring unit (Visualsonics, Toronto, Ontario, Canada). Mice were kept under anesthesia for the duration of the experiment. After the mouse was completely anesthetized, the tail vein was catheterized using a modified 27-gauge, 1/2-inch butterfly catheter (Terumo Medical Corporation, Somerset, NJ). Prior to catheterization, the tubing was removed from the butterfly catheters and replaced with smaller 27-gauge Tygon® tubing (0.015" inner-diameter, Cole-Parmer, Vernon Hills, IL). The mouse was then shaved in the kidney region. A Vevo 770 small animal ultrasound imaging scanner with a 40-MHz imaging transducer was placed over the kidney region and coupled using Aquasonic-100 ultrasound transmission gel (Parker Laboratories, Fairfield, NJ). A bolus injection of 100 μL of microbubble suspension (concentrations range from 1×10^6 to 1×10^8 MB/bolus) was injected while imaging continuously at 16 frames per second. At the focal length (6 mm), the peak negative pressure is 3.49 MPa with an acoustic power of 0.017 mW and a mechanical index of 0.57. In the current work, the transmit power setting was set to 79%, corresponding to 1 dB attenuation of the signal. These acoustic parameters were reported by the manufacturer (Visualsonics) from measurements made in water and adjusted with a derating factor of $0.3 \text{ dB cm}^{-1} \text{ MHz}^{-1}$. Mice were injected with size-selected microbubble populations of 1-2 μm , 4-5 μm , or 6-8 μm at specific number concentrations ranging between 1×10^6 and 1×10^8 MB/bolus ($n = 4-7$ per group). Respiratory gating was used to synchronize data acquisition with the mouse respiratory cycle in order to reduce motion artifact during image analysis. Respiratory gating lowered the effective acquisition rate to 2 frames per second. Ultrasound imaging was performed from 0-5 minutes. For longer circulating bubbles, imaging was performed from 0-20 minutes following injection of the microbubble solution. Mice were given up to three injections per imaging session (20 minutes was given between start points of the injections) and then removed from anesthesia. After the mouse regained consciousness, it was returned to its cage.

Data analysis

Image analysis of the contrast enhancement was performed using the mean grayscale video intensity determined by integrating the pixel intensity values over a specific region of interest (ROI) in every acquired frame. The ROI was selected in the upper portion of the kidney to minimize effects of signal attenuation and shadowing. The log-compressed grayscale video intensity values were linearized using the Vevo770 application software (Visualsonics). This method was performed by characterization of input/output relationship of the 40 MHz transducer to calculate the input voltage from the grayscale pixel values. The relationship between the grayscale value and input voltage is given as:

$$y = m \ln(x) + b$$

where y is the grayscale value and x is the input voltage. The slope m and offset b were determined to be 369.39 and 371.86, respectively. The details regarding the validation of this method can be found in the VSI White paper (available through Visualsonics). The linearized data were baseline adjusted and plotted using Prism 5 graphing software (Graphpad Software, La Jolla, CA).

The amplitude, persistence half-life, decay rate and total integrated signal enhancement (area under the curve; AUC) of the contrast signal was measured by fitting the data to a drug persistence model, in which agent is absorbed at a first-order rate into the intravascular compartment, mixes immediately and then decays at a first-order rate, as described by Saltzman (Saltzman 2001). See Appendix for details. TIC data were fit to the pharmacokinetic model using a least-squares regression algorithm. All statistical analyses were performed using Prism 5 software.

Results

Microbubble Size Distribution

Figure 1 shows the number- and volume-weighted size distributions from freshly made microbubble suspensions formulated by vial shaking and probe sonication. Both methods resulted in microbubbles with multi-modal size distributions, as previously reported (Feshitan et al. 2009), with diameters ranging from 0.5 μm to 10 μm in diameter. The number-weighted size distributions showed that most (>95%) of the microbubbles are smaller than 2 μm diameter. The volume-weighted distributions showed that sub-populations of microbubbles existed at distinct size ranges (specifically at 1-2 μm , 4-5 μm and 6-8 μm diameter), as indicated by the peaks.

The size-isolation technique developed by Feshitan et al. (Feshitan et al. 2009) was used to separate microbubbles at 1-2 μm , 4-5 μm and 6-8 μm size ranges in high concentrations (10^7 to 10^9 MB/mL). Figure 2 shows representative number- and volume-weighted size distributions for the size-selected microbubble populations used in this study. Differential centrifugation allowed rapid and efficient isolation of size-selected microbubbles with monomodal distributions and relatively low polydispersity in comparison to the original suspension.

High Frequency In Vivo Imaging

All mice were given 100- μL bolus injections ranging from 10^6 to 10^8 microbubbles total. Imaging was performed above the left kidney of the mouse using a 40-MHz ultrasound transducer to record ultrasound videos in fundamental mode. Figure 3 shows typical grayscale images of the mouse kidney before and after a bolus injection of 5×10^7 microbubbles for

polydisperse and size-selected microbubbles. The images were taken at the peak amplitude of the signal, typically 30-60 seconds after the bolus injection was given. Contrast detection software (Visualsonics), which colors the positive contrast-enhanced pixels in green, was used to highlight the presence of microbubbles.

The 1-2 μm bubble population showed little increase in the grayscale video intensity after the bolus injection (Figure 3B2), compared to a typical polydisperse sample (Figure 3A2). Contrast detection software indicated sparse signal increase throughout the kidney except in large blood vessels ($>100 \mu\text{m}$ in diameter). However, attenuation of the ultrasound signal was observed in the lower portion of the kidney and below.

The 4-5 μm bubble population showed a noticeable increase in the brightness and speckling throughout the kidney after the bolus injection (Figure 3C2), compared to background images prior to the injection. Contrast detection software similarly indicated a higher level of contrast enhancement (indicated by the area and intensity of green color) following injections of the 4-5 μm bubbles, compared to injections of the 1-2 μm bubbles.

The 6-8 μm bubble population showed the largest increase in brightness and speckling following the bolus injection (Figure 3D2). The contrast detection software also indicated higher levels of contrast enhancement from the 6-8 μm bubbles compared to both 4-5 μm and 1-2 μm bubbles. The 6-8 μm microbubbles consistently gave the most intense and longest lasting positive contrast enhancement.

The levels of contrast enhancement and persistence of the contrast agent in the blood stream were analyzed from the time-intensity curves (TIC) for each of the size-selected microbubble populations. Typically, the time-intensity curves were generated by integrating the image pixel intensities over a region of interest in the upper portion of the kidney (Figs. 3-4). The upper portion was selected to minimize effects of microbubble-induced attenuation and shadowing, particularly at higher microbubble concentrations. Interestingly, the 1-2 μm bubble population did not show a measurable signal increase above noise when evaluating the mean video intensity in the upper portion of the kidney (Figure 4B). A small amount of signal enhancement was observed qualitatively, but could not be accurately quantified due to a very low signal-to-noise ratio. However, the presence of microbubbles in circulation was detectable by attenuation of the signal (Figure 4C). By selecting an ROI that encompassed the entire kidney, a decrease in the mean video intensity was observed (Figure 4C), and the circulation persistence of the 1-2 μm bubbles could be measured.

Figure 5 shows typical TIC's generated from individual bolus injections of 5×10^7 MB for each size-selected population. Injections of 4-5 μm and 6-8 μm bubbles significantly enhanced the video intensity compared to both 1-2 μm bubbles and polydisperse samples injected at the same number concentration. Larger 4-5 μm and 6-8 μm microbubbles were observed to persist longer in circulation than 1-2 μm and polydisperse bubbles.

Pharmacokinetic Model

A pharmacokinetic model was used further analyze the TIC data in order to determine the signal amplitude and contrast persistence half-life over a range of microbubble concentrations (10^6 to 10^8 MB/bolus) for each of the size-selected microbubble populations (Figure 6). The model assumes a first-order rate of bolus spreading following injection, uniform distribution of the microbubbles in circulation, and a first-order rate of elimination of the microbubbles from circulation. While these assumptions may not fully describe the kinetics of microbubble influx and elimination, the model fits the data well (typical $R^2 > 0.90$) and allows parameters such as the maximum signal intensity and half-life to be quantified.

Attenuation of the signal from 1-2 μm bubbles was only detectable above 5×10^7 MB/bolus. The change in signal intensity was greater at 1×10^8 MB/bolus (-128 ± 44 relative units (R.U.)) compared to 5×10^7 MB/bolus (-94 ± 32 R.U.), but the change was not statistically different ($p = 0.23$), as determined by a Students' t-test. The half-life of the 1-2 μm bubbles significantly increased, however, from 51 ± 22 seconds to 115 ± 24 seconds ($p < 0.05$).

The 4-5 μm bubble population showed a positive signal enhancement for concentrations ranging from 5×10^6 to 1×10^8 MB/bolus. Both signal amplitude and persistence time increased with microbubble concentration. The signal amplitude increased from 82 ± 33 R.U. at the lowest concentration of 5×10^6 MB/bolus to 4081 ± 1575 R.U. at the highest concentration of 1×10^8 MB/bolus. Similarly, the persistence half-life increased from 66 ± 9 seconds to 117 ± 21 seconds for injections of 5×10^6 and 1×10^8 MB/bolus. The signal amplitude and contrast persistence were significantly different for each concentration ($p < 0.05$).

Similarly, the 6-8 μm bubble population showed a positive signal enhancement for concentrations ranging 1×10^6 to 5×10^7 MB/bolus. As with the 4-5 μm bubbles, both signal amplitude and persistence time increased with microbubble concentration. The signal amplitude increased from 82 ± 31 R.U. at the lowest concentration of 1×10^6 MB/bolus to 1886 ± 993 R.U. at the highest concentration of 5×10^7 MB/bolus. The half-life increased from 119 ± 31 seconds to 350 ± 84 seconds for injections of 1×10^6 and 5×10^7 MB/bolus. Interestingly, one-way ANOVA determined that there was no significant change in the persistence half-life for concentrations ranging from 1×10^6 to 1×10^7 MB/bolus ($p = 0.62$). However, bolus injections of 5×10^7 bubbles showed a dramatic increase (3-fold) in the persistence half-life compared with the lower concentrations ($p < 0.01$).

The signal intensities and contrast persistence times were compared between the individual size populations as well. At the highest comparable concentration of 5×10^7 MB/bolus, the 6-8 μm bubbles demonstrated a 5.4-fold increase in the signal intensity compared to the 4-5 μm bubbles ($p < 0.01$). At 1×10^7 and 5×10^6 MB/bolus, there was no statistical difference in the signal intensities between the 4-5 μm and 6-8 μm bubbles ($p = 0.23$ and 0.10 , respectively). Concentrations greater than 5×10^7 MB/bolus for the 6-8 μm bubbles were difficult to achieve owing to the small population of the microbubbles in the initial suspension.

The signal half-life from the 6-8 μm bubbles was significantly longer than the 4-5 μm and 1-2 μm populations for every comparable concentration ($p < 0.01$). At the highest comparable concentration of 5×10^7 MB/bolus, the half-life of the 6-8 μm bubbles was 350 ± 84 seconds, which was 4-fold longer than the 4-5 μm bubbles, and 7-fold longer than the 1-2 μm bubbles. The signal from the 4-5 μm bubbles did not have a significantly longer half-life than the 1-2 μm bubbles at 5×10^8 MB/bolus ($p = 0.08$), or at 1×10^8 MB/bolus ($p = 0.14$).

The effect of the total gas volume injected on the signal amplitude and half-life was explored. Total injected gas volume was determined by the size distribution and the total number of bubbles (Figure 7). The total gas volume injected for the highest concentration of 1-2 μm bubbles ($0.17 \mu\text{L}$ at 10^8 MB/bolus) was moderately less than the volume injected for the lowest concentrations of 4-5 μm ($0.23 \mu\text{L}$ at 5×10^7 MB/bolus) and 6-8 μm ($0.18 \mu\text{L} \mu\text{m}^3$ at 10^6 MB/bolus), but of the same order of magnitude. At these microbubble concentrations, the signal from the 1-2 μm bubbles mainly attenuated without producing a measurable increase in the video signal, whereas 4-5 μm and 6-8 μm bubbles demonstrated a clear signal enhancement (Fig. 7A). The relationship between gas volume and signal amplitude was nonlinear, particularly for 4-5 μm bubbles, indicating the onset of multiple scattering events at the higher microbubble concentrations (Soetanto and Chan 2000; Chen and Zhu 2006).

At the equivalent gas volume ($\sim 0.2 \mu\text{L}$), the half-life of 1-2, 4-5 and 6-8 μm bubbles was 135 ± 65 , 56 ± 34 and 106 ± 27 seconds, respectively. These values are remarkably similar, although

the nearly 2-fold longer half-life for 1-2 μm and 6-8 μm versus 4-5 μm bubbles was statistically significant ($p < 0.01$). The shorter half-life for 4-5 μm bubbles is likely due to an underestimation from the method of analysis, as discussed below. The relationship between gas volume and signal half-life had a moderate linear correlation ($R^2 = 0.75$).

The parameters D_0 , k_1 , k_2 , and the AUC are shown in Figure 8. The D_0 parameter (Figure 8A) is directly related to the maximum signal intensity. The D_0 values estimated by the model fit showed an identical trend to the maximum signal amplitudes shown in Figure 6A.

The k_1 parameter (Figure 8B) is a measure of the influx rate of contrast agent into the kidney, which depends on the injection and bolus spreading. No trend was observed for any of the size-selected microbubble populations with increasing concentration. For example, the effect of increasing microbubble concentration for 4-5 and 6-8 μm bubbles was analyzed using one-way ANOVA. No statistical difference in the mean k_1 values with increasing microbubble concentration was found ($p = 0.21$ and $p = 0.32$, respectively).

The k_2 parameter (Figure 8C) is a measure of the decay of contrast agent in the circulation. The mean k_2 values were significantly lower for the 6-8 μm bubble compared to the 4-5 μm and 1-2 μm bubbles at equivalent concentrations ($p < 0.01$). No statistical difference was observed between mean k_2 values for 4-5 μm and 1-2 μm bubbles at any comparable concentration.

The AUC parameter is a measure of the total integrated signal enhancement and is the most relevant measure of the capability of the microbubbles to produce contrast. The AUC was determined to be significantly higher for the 6-8 μm bubbles than for the 4-5 μm bubbles at equivalent concentrations ($p < 0.01$). For example, at the highest concentration of 6-8 μm bubbles injected, the mean AUC was 16-fold higher than the mean AUC for the 4-5 μm bubbles at the same concentration. The AUC of 1-2 μm bubbles are shown as negative values due to the attenuation of the signal.

Discussion

In vivo imaging of the size-selected microbubble populations illustrated that larger microbubbles ($> 4 \mu\text{m}$ diameter) enhanced the video signal more effectively at 40 MHz than smaller bubbles in fundamental imaging mode. Small bubbles, between 1-2 μm in size, minimally enhanced the ultrasound signal in the mouse kidney, but they strongly attenuated (Figures 3-5). This result is consistent with theoretical predictions, in which smaller microbubbles are expected to absorb HFU to a greater degree than they scatter at the fundamental frequency (Chan et al. 1997).

To gain physical insight into our *in vivo* imaging data, we calculated the relative contributions of the scattering cross section (σ_s) and absorption cross section (σ_a) to the extinction (attenuation) cross section (σ_e at 40 MHz as a function of microbubble size. Our estimates are based on Rayleigh-Plesset theory developed by Medwin (Medwin 1977) with an additional damping coefficient due to frictional loss added by de Jong et al. (de Jong et al. 1992; de Jong and Hoff 1993). The equations and parameters used in the calculations are given in the Appendix. Results are shown in Figure 9A. Larger microbubbles are predicted to produce more scattering and less absorption. The amount of scattering predicted for a 4-5 μm bubble is 5-fold higher than for a 1-2 μm bubble, while that for a 6-8 μm bubble is 10-fold higher than for a 1-2 μm bubble. At microbubble diameters between 1 and 2 μm , the model predicts energy loss primarily owing to absorption of the ultrasound signal. Loss of energy at the fundamental due to absorption effectively reduces the scattering-to-attenuation ratio (STAR), a value that was developed to describe the efficiency of microbubble contrast agents to enhance

visualization in tissue (Bouakaz et al. 1998a). For small microbubbles close to 1 μm in diameter, it is estimated from Figure 9A that 50% of the attenuation is due to absorption (Fig. 9).

Note that resonant microbubbles are more efficient scatterers when volume-fraction matched (Medwin 1977; de Jong et al. 1992; de Jong and Hoff 1993). The 1-2 μm bubbles are nearest the resonant peak at 40 MHz (Fig. 9), but they are not resonant, which limits our conclusions. The result remains, however, that larger microbubbles provide greater contrast enhancement when imaging at depth, which is dominated by the STAR effect.

Other experimental factors may explain to the inability of the 1-2 μm bubbles to measurably enhance the video intensity. It is possible that an increase in the video signal may become discernable from noise by increasing the applied ultrasound amplitude or imaging alternate tissue. Interestingly, it was observed that 1-2 μm bubbles showed a significant increase in video intensity in the large blood vessels (>100 μm in diameter) of the kidney. These large blood vessels were characterized by dark circles within the kidney that became significantly brighter following the bolus injection of 1-2 μm bubbles.

However, it is unlikely that the lower enhancement (shadowing) observed for smaller microbubbles is simply a consequence of larger numbers reaching the kidney region. At each matched number concentration (1×10^6 to 1×10^8 MB/mL), the larger microbubbles consistently showed greater contrast enhancement and longer circulation persistence (Fig. 6). We did not observe a rise and then drop in enhancement with increasing dose for any of the sizes. Furthermore, the results are in line with theory, which predicts a lower STAR value for the smaller microbubbles (Fig. 9).

We also investigated the effect of surface tension on the model predictions. The extinction cross section of microbubbles at 40 MHz was calculated as a function of microbubble radius for negligible (0 mN/m) and high (72 mN/m) surface tension. Figure 9B shows that surface tension had little effect on attenuation of the acoustic signal. This analysis does not preclude other effects of the lipid shell, such as surface dilatational viscoelasticity.

The absolute change in contrast increased with microbubble concentration for all sizes. A concentration-dependent increase in signal amplitude was previously demonstrated for non-linear HFU by Stapleton et al. (Stapleton et al. 2009) using polydisperse Definity microbubbles. An increase in backscatter has also been observed with increasing microbubble concentration at lower ultrasound frequencies (Marsh et al. 1999). However, while increasing concentration enhanced contrast in the upper region of the kidney, it also enhanced attenuation and shadowing in the lower region of the kidney. Therefore, microbubble concentration must be carefully titrated to provide the desired enhancement at a specific imaging depth.

The lowest total gas volumes injected for the 4-5 μm and 6-8 μm bubbles were nearly the same as the highest concentration injected for the 1-2 μm bubbles ($\sim 0.2 \mu\text{L}$). Both 4-5 μm and 6-8 μm bubbles showed a positive contrast enhancement, whereas the 1-2 μm mainly attenuated the signal, indicating that the amount of contrast enhancement is not determined by the volume of the gas that is injected, but rather how the gas is distributed within the microbubbles.

The time-intensity curves (TIC's) of the size-selected microbubbles indicate that larger microbubbles unexpectedly persist longer in the blood stream, especially at high concentrations. Clearance of the microbubbles from circulation has been attributed to (1) filtering of microbubbles by the lung and spleen, (2) dissolution of the microbubble gas core, and (3) removal by macrophages in the lungs liver and spleen. Filtering of the microbubbles and macrophage clearance predict that larger microbubbles would be removed more rapidly. Based on the longer contrast persistence of larger bubbles, it can be inferred that dissolution of the gas core is the dominant mechanism of contrast decay. We suggest that larger

microbubbles may deform to traverse the capillary beds without becoming lodged and occluding flow. Microbubble deformation has previously been observed both *in vitro* and *in vivo* (Lindner et al. 2002; Rychak et al. 2006).

At the only comparable gas volume concentration ($\sim 0.2 \mu\text{L}$), the 1-2, 4-5 and 6-8 μm diameter microbubbles had similar persistence half-lives. This result is consistent with gas dissolution as the primary mechanism of contrast decay. Contrast elimination was further explored by fitting the TIC data to a pharmacokinetic model and evaluating the k_2 parameter (Figure 8C). The k_2 parameter was significantly lower for the 6-8 μm bubbles than 1-2 μm or 4-5 μm bubbles. However, no significant differences were observed between 1-2 μm and 4-5 μm bubbles at comparable number concentrations. Again, this is consistent with dissolution as the main mechanism for contrast decay. It is likely that the persistence of 4-5 μm bubbles was underestimated by this analysis, since they dissolved into 1-2 μm bubbles, with low STAR values, and thus became difficult to detect by enhancement of the upper region of the kidney (compared to attenuation of the entire kidney, as measured for 1-2 μm bubbles). The 6-8 μm bubbles, on the other hand, dissolved into signal-enhancing 4-5 μm bubbles before they dissolved into signal-attenuating 1-2 μm bubbles.

Conclusion

Using the technique of differential centrifugation, we isolated microbubbles of distinct size populations and determined their acoustic imaging impact *in vivo*. The acoustic and pharmacokinetic behavior of 1-2, 4-5 and 6-8 μm diameter microbubbles were measured in the mouse kidney using 40-MHz fundamental-mode imaging. Interestingly, small 1-2 μm diameter microbubbles did not produce a noticeable contrast enhancement compared to tissue at any concentration. In fact, 1-2 μm bubbles mainly attenuated the ultrasound signal of the mouse kidney. This observation was in agreement with predictions of the scattering and absorption cross sections that predicted 1-2 μm bubbles would have a low STAR at 40 MHz. Larger microbubbles ($> 4 \mu\text{m}$), on the other hand, were highly echogenic and persisted longer in the mouse circulation. The largest microbubbles (6-8 μm) produced a detectable signal even at very low microbubble concentrations (10^6 MB/bolus). 6-8 μm bubbles had the longest persistence, lasting more than 15 minutes in circulation at the highest concentrations (5×10^7 MB/bolus).

It is important to note that the size distributions of the microbubbles are likely to evolve immediately following the bolus injection, which has not been addressed in this study. For example, changes in temperature, pressure and ambient gas concentrations may impact microbubble size when delivered *in vivo*. The size change of the microbubbles following the bolus injections is a complex issue. While an increase in temperature from 25 to 37 $^\circ\text{C}$ can cause a slight increase in volume of the microbubbles (a maximum increase in volume by a factor of 1.04 assuming ideal gas law and no change in internal pressure), other factors such as gas influx into the core and microbubble dissolution can have a more dramatic impact on the microbubble size following injection (Kwan and Borden 2010). Regardless, we found that the larger microbubbles circulated longer with no adverse effects observed in the mice following the imaging protocol, indicating they are not growing upon injection and lodging in capillaries.

Commercially available ultrasound contrast agents, such as Definity (Lantheus Medical Imaging) and SonoVue (Bracco), typically comprise a majority of microbubbles below 2 μm diameter (Schneider 1999; Gorce et al. 2000; Goertz et al. 2007; Stapleton et al. 2009). Our results indicate that a very small percentage of the microbubbles (those larger than 2 μm diameter) in these formulations are contributing most to the contrast enhancement. The more numerous, smaller microbubbles actually reduce contrast. Therefore, an optimized contrast

formulation for fundamental mode FUS imaging would comprise larger microbubbles. The effect of microbubble size on non-linear mode FUS remains to be determined.

Acknowledgments

We wish to gratefully acknowledge Dr. Peter Frinking from Bracco Research for an insightful discussion. This research was supported by NIH R01-EB009066 and R21-CA139173 to MAB.

Appendix

A. Pharmacokinetic model for contrast persistence

The pharmacokinetic model used to fit contrast time-intensity curves was given by Saltzman (Saltzman 2001):

$$\frac{C}{D_0} = \frac{k_1}{(k_2 - k_1)(e^{-k_1 t} - e^{-k_2 t})} \quad (1)$$

where C is the relative amount of measured contrast enhancement, D_0 is the initial amount of contrast, k_1 is a pseudo-first-order rate constant describing the influx of contrast into the system, and k_2 is a pseudo-first-order rate constant describing the elimination of contrast from the system.

B. Estimation of the extinction cross-section

The extinction cross section was given previously in the literature (Medwin 1977; de Jong et al. 1992; de Jong and Hoff 1993):

$$\sigma_e = \sigma_s + \sigma_a \quad (2)$$

The extinction cross-section (σ_e) is the total energy of the ultrasound beam lost when passing through the microbubble-containing medium and is defined by the sum of the scattering cross-section (σ_s) and absorption cross-section (σ_a) of the microbubbles. The scattering and absorption cross sections of the bubble are given as:

$$\sigma_s = \frac{4\pi r^2}{\left(\frac{f}{f_r} - 1\right)^2 + \delta^2} \quad (3)$$

$$\sigma_a = \sigma_s \left(\frac{\delta}{\delta_r} - 1 \right) \quad (4)$$

Where r is the microbubble radius, f_r is the resonance frequency of the microbubble, f is the driving frequency of the acoustic pulse, δ is the overall damping coefficient, and δ_r is the damping coefficient for re-radiation. It should be cautioned that at 40 MHz the ultrasound wavelength begins to approach the size of the microbubbles tested in this study. However, the theory does provide some physical insight into the experimental results.

The resonance frequency f_r is defined given as:

$$f_r = f_{RA} (b\xi)^{\frac{1}{2}} + \frac{1}{2\pi} \left(\frac{S_{shell}}{m} \right)^{\frac{1}{2}} \quad (5)$$

where f_{RA} from equation (5) is the natural frequency of the free oscillation, ζ is a substitution variable, b is a dimensionless stiffness factor, S_{shell} is the shell stiffness and m is the effective mass. Total damping (δ) is a sum of the re-radiation (δ_r), shear viscous losses in the surrounding medium (δ_v), thermal transport between the gas and liquid (δ_T), and frictional damping (δ_F).

$$\delta = \delta_r + \delta_v + \delta_T + \delta_F \quad (6)$$

C. Estimation of the bubble resonance frequency

The natural frequency of the free oscillation given as:

$$f_{RA} = \frac{1}{2\pi r} \left(\frac{3\gamma P_0}{\rho} \right)^{\frac{1}{2}} \quad (7)$$

where P_0 is the ambient pressure, ρ is the density of the liquid, and γ is the ratio of constant-volume specific heat to constant-pressure specific heat. ζ from equation (5) is a substitution factor defined as:

$$\xi = 1 + \frac{2\beta}{P_0 r} \left[1 - \frac{1}{3\gamma b} \right] \quad (8)$$

Where β is the surface tension and b is defined by:

$$b = \left(1 + B(\omega, r)^2 \right)^{-1} \left[1 + \frac{3(\gamma - 1)}{X} \left(\frac{\sinh X + \sin X}{\cosh X - \cos X} \right) \right]^{-1} \quad (9)$$

where $B(\omega, r)$ and X are defined by equations (13) and (14) respectively.

D. Estimation of the damping coefficients

Re-radiation (δ_r) is defined as:

$$\delta_r = kr \quad (10)$$

where k is the wave number. Viscous damping (δ_v) is defined as:

$$\delta_v = 4 \frac{\eta}{\rho \omega r^2} \quad (11)$$

where η is the viscosity of the liquid, ρ is the density of the liquid and ω is the applied angular frequency. Thermal damping (δ_T) is defined by:

$$\delta_r = B(\omega, r) \frac{\omega_r^2}{\omega^2} \quad (12)$$

where $B(\omega, r)$ is defined as:

$$B(\omega, r) = 3(\gamma - 1) \left[\frac{X(\sinh X + \sin X) - 2(\cosh X - \cos X)}{X^2(\cosh X - \cos X) + 3(\gamma - 1)X(\sinh X + \sin X)} \right] \quad (13)$$

and X is defined by:

$$X = r \left(\frac{2\omega\rho_g C_{pg}}{K_g} \right)^{\frac{1}{2}} \quad (14)$$

where C_p is the constant-pressure specific heat, K_g is the thermal conductivity of the gas, and ρ_g is the gas density defined by:

$$\rho_g = \rho_{gA} \left[1 + \frac{2\beta}{P_0 r} \right] \quad (15)$$

where ρ_{gA} is the gas density at ambient pressure, β is the surface tension and P_0 is the ambient pressure. The angular resonance frequency in equation (12) is defined by:

$$\omega_r^2 = \omega_{rg}^2 + \frac{S_{\text{shell}}}{m} \quad (16)$$

where ω_{rg}^2 is the angular resonance frequency of an ideal gas bubble defined as:

$$\omega_{rg}^2 = \frac{S_a}{m} b\beta \quad (17)$$

where S_a is the adiabatic stiffness of the gas defined as:

$$S_a = 12\pi\gamma P_0 r \quad (18)$$

where γ is ratio of constant-volume specific heat to constant-pressure specific heat. Frictional damping (δ_F) is defined by:

$$\delta_F = \frac{S_f}{\omega m} \quad (19)$$

where S_f is the shell friction coefficient.

Table A.1
Parameters used to estimate scattering and adsorption cross sections

Parameters	
f - Frequency [MHz]	40
$\gamma = C_v/C_p$ (Smith 2001)	1.3
Speed of Sound [m/s]	1497
P_0 - Ambient Pressure [Pa]	101325
P - Density of Water [kg/m ³]	1000
C_{pg} - Heat Capacity [J/K] (Yaws 2009)	406.51
P_{gA} - Ambient density of PFB [kg/m ³] (Ideal)	9.7
K_g - Thermal Conductivity of PFB [W/(m K)] (Yaws 2003)	0.0143
S_f - Shell friction damping coefficient [kg/s] x 10 ⁻⁸	1
S_{shell} - Shell Stiffness [N/m] (Gorce 2000)	27
η - Viscosity of water [Pa s] x 10 ⁻⁴	6.92
S_a - Gas Stiffness [N/m] (Medwin 1977)	24.829
σ - Surface Tension [mK/m]	0 - 72

References

- Borden MA, Longo ML. Dissolution Behavior of Lipid Monolayer-Coated, Air-Filled Microbubbles: % Effect of Lipid Hydrophobic Chain Length. *Langmuir* 2002;18:9225–33.
- Borden MA, Longo ML. Oxygen permeability of fully condensed lipid monolayers. *J Phys Chem B* 2004;108:6009–16.
- Bouakaz A, De Jong N, Cachard C. Standard properties of ultrasound contrast agents. *Ultrasound Med Biol* 1998a;24:469–72. [PubMed: 9588001]
- Bouakaz A, de Jong N, Cachard C, Jouini K. On the effect of lung filtering and cardiac pressure on the standard properties of ultrasound contrast agent. *Ultrasonics* 1998b;36:703–8. [PubMed: 9651600]
- Chan M, Soetanto K, Okujima M. Simulations of Contrast Effects from Free Microbubbles in Relation to Their Size, Concentration and Acoustic Properties. *Jpn J Appl Phys* 1997;36:3.
- Chen J, Zhu Z. Ultrasound attenuation in encapsulated microbubble suspensions: The multiple scattering effects. *Ultrasound Med Biol* 2006;32:961–9. [PubMed: 16785017]
- Coatney RW. Ultrasound imaging: principles and applications in rodent research. *ILAR J* 2001;42:233–47. [PubMed: 11406722]
- Dayton PA, Ferrara KW. Targeted imaging using ultrasound. *Journal of Magnetic Resonance Imaging* 2002;16:362–77. [PubMed: 12353252]
- de Jong N, Hoff L. Ultrasound scattering properties of Albunex microspheres. *Ultrasonics* 1993;31:175–81. [PubMed: 8484195]
- de Jong N, Hoff L, Skotland T, Bom N. Absorption and scatter of encapsulated gas filled microspheres: theoretical considerations and some measurements. *Ultrasonics* 1992;30:95–103. [PubMed: 1557838]
- Epstein PS, Plesset MS. On the Stability of Gas Bubbles in Liquid-Gas Solutions. *The Journal of Chemical Physics* 1950;18:1505–9.
- Ferrara KW, Borden MA, Zhang H. Lipid-shelled vehicles: engineering for ultrasound molecular imaging and drug delivery. *Acc Chem Res* 2009;42:881–92. [PubMed: 19552457]
- Feshitan JA, Chen CC, Kwan JJ, Borden MA. Microbubble size isolation by differential centrifugation. *J Colloid Interface Sci* 2009;329:316–24. [PubMed: 18950786]

- Foster FS, Burns PN, Simpson DH, Wilson SR, Christopher DA, Goertz DE. Ultrasound for the visualization and quantification of tumor microcirculation. *Cancer Metastasis Rev* 2000a;19:131–8. [PubMed: 11191052]
- Foster FS, Mehi J, Lukacs M, Hirson D, White C, Chaggares C, Needles A. A new 15-50 MHz array-based micro-ultrasound scanner for preclinical imaging. *Ultrasound Med Biol* 2009;35:1700–8. [PubMed: 19647922]
- Foster FS, Pavlin CJ, Harasiewicz KA, Christopher DA, Turnbull DH. Advances in ultrasound biomicroscopy. *Ultrasound Med Biol* 2000b;26:1–27. [PubMed: 10687788]
- Foster FS, Zhang MY, Zhou YQ, Liu G, Mehi J, Cherin E, Harasiewicz KA, Starkoski BG, Zan L, Knapik DA, Adamson SL. A new ultrasound instrument for in vivo microimaging of mice. *Ultrasound Med Biol* 2002;28:1165–72. [PubMed: 12401387]
- Goertz DE, de Jong N, van der Steen AF. Attenuation and size distribution measurements of Definity and manipulated Definity populations. *Ultrasound Med Biol* 2007;33:1376–88. [PubMed: 17521801]
- Gorce JM, Arditi M, Schneider M. Influence of bubble size distribution on the echogenicity of ultrasound contrast agents: a study of SonoVue. *Invest Radiol* 2000;35:661–71. [PubMed: 11110302]
- Jugold M, Palmowski M, Huppert J, Woenne EC, Mueller MM, Semmler W, Kiessling F. Volumetric high-frequency Doppler ultrasound enables the assessment of early antiangiogenic therapy effects on tumor xenografts in nude mice. *Eur Radiol* 2008;18:753–8. [PubMed: 18084768]
- Kabalnov A, Klein D, Pelura T, Schutt E, Weers J. Dissolution of multicomponent microbubbles in the bloodstream: 1. Theory. *Ultrasound Med Biol* 1998;24:739–49. [PubMed: 9695277]
- Kamaev PP, Hutcheson JD, Wilson ML, Prausnitz MR. Quantification of optison bubble size and lifetime during sonication dominant role of secondary cavitation bubbles causing acoustic bioeffects. *J Acoust Soc Am* 2004;115:1818–25. [PubMed: 15101659]
- Klibanov AL. Microbubble contrast agents: targeted ultrasound imaging and ultrasound-assisted drug-delivery applications. *Invest Radiol* 2006;41:354–62. [PubMed: 16481920]
- Klibanov AL. Ultrasound molecular imaging with targeted microbubble contrast agents. *Journal of Nuclear Cardiology* 2007;14:876–84. [PubMed: 18022115]
- Kwan JJ, Borden MA. Microbubble dissolution in a multigas environment. *Langmuir*. 2010 Article ASAP.
- Lindner JR, Dayton PA, Coggins MP, Ley K, Song J, Ferrara K, Kaul S. Noninvasive imaging of inflammation by ultrasound detection of phagocytosed microbubbles. *Circulation* 2000a;102:531–8. [PubMed: 10920065]
- Lindner JR, Song J, Jayaweera AR, Sklenar J, Kaul S. Microvascular rheology of definity microbubbles after intra-arterial and intravenous administration. *Journal of the American Society of Echocardiography* 2002;15:396–403. [PubMed: 12019422]
- Lindner JR, Song J, Xu F, Klibanov AL, Singbartl K, Ley K, Kaul S. Noninvasive ultrasound imaging of inflammation using microbubbles targeted to activated leukocytes. *Circulation* 2000b;102:2745–50. [PubMed: 11094042]
- Marsh JN, Hughes MS, Brandenburger GH, Miller JG. Broadband measurement of the scattering-to-attenuation ratio for Albunex at 37 degrees C. *Ultrasound Med Biol* 1999;25:1321–4. [PubMed: 10576274]
- Medwin H. Counting Bubbles Acoustically - Review. *Ultrasonics* 1977;15:7–13.
- Migaleddu V, Scanu AM, Quaia E, Rocca PC, Dore MP, Scanu D, Azzali L, Virgilio G. Contrast-enhanced ultrasonographic evaluation of inflammatory activity in Crohn's disease. *Gastroenterology* 2009;137:43–52. [PubMed: 19422826]
- Moghimi SM. MECHANISMS OF SPLENIC CLEARANCE OF BLOOD-CELLS AND PARTICLES - TOWARDS DEVELOPMENT OF NEW SPLENOTROPIC AGENTS. *Adv Drug Delivery Rev* 1995;17:103–15.
- Moghimi SM, Hunter AC, Murray JC. Long-circulating and target-specific nanoparticles: Theory to practice. *Pharmacological Reviews* 2001;53:283–318. [PubMed: 11356986]
- Palmowski M, Huppert J, Hauff P, Reinhardt M, Schreiner K, Socher MA, Hallscheidt P, Kauffmann GW, Semmler W, Kiessling F. Vessel fractions in tumor xenografts depicted by flow- or contrast-sensitive three-dimensional high-frequency Doppler ultrasound respond differently to antiangiogenic treatment. *Cancer Res* 2008;68:7042–9. [PubMed: 18757418]

- Rychak JJ, Lindner JR, Ley K, Klivanov AL. Deformable gas-filled microbubbles targeted to P-selectin. *Journal Of Controlled Release* 2006;114:288–99. [PubMed: 16887229]
- Saltzman, M. *Drug Delivery: Engineering Principles for Drug Therapy*. Oxford University Press; 2001.
- Sarkar K, Katiyar A, Jain P. Growth and dissolution of an encapsulated contrast microbubble: effects of encapsulation permeability. *Ultrasound Med Biol* 2009;35:1385–96. [PubMed: 19616160]
- Schneider M. Characteristics of SonoVue trade mark. *Echocardiography* 1999;16:743–6. [PubMed: 11175217]
- Short AC, Montoya ML, Gebb SA, Presson RG, Wagner WW, Capen RL. Pulmonary capillary diameters and recruitment characteristics in subpleural and interior networks. *Journal of Applied Physiology* 1996;80:1568–73. [PubMed: 8727541]
- Smith, JM.; Van Ness, HC.; Abbott, MM. *Introduction to Chemical Engineering Thermodynamics*. 2001.
- Soetanto K, Chan M. Fundamental studies on contrast images from different-sized microbubbles: analytical and experimental studies. *Ultrasound Med Biol* 2000;26:81–91. [PubMed: 10687796]
- Stapleton S, Goodman H, Zhou YQ, Cherin E, Henkelman RM, Burns PN, Foster FS. Acoustic and kinetic behaviour of definity in mice exposed to high frequency ultrasound. *Ultrasound Med Biol* 2009;35:296–307. [PubMed: 18950930]
- Tartis MS, Kruse DE, Zheng HR, Zhang H, Kheirloom A, Marik J, Ferrara KW. Dynamic microPET imaging of ultrasound contrast agents and lipid delivery. *Journal of Controlled Release* 2008;131:160–6. [PubMed: 18718854]
- Willmann JK, Cheng Z, Davis C, Lutz AM, Schipper ML, Nielsen CH, Gambhir SS. Targeted microbubbles for imaging tumor angiogenesis: Assessment of whole-body biodistribution with dynamic micro-PET in mice. *Radiology* 2008;249:212–9. [PubMed: 18695212]
- Yaws, CL. *Yaws' Handbook of Thermodynamic and Physical Properties of Chemical Compounds*. 2003.
- Yaws, CL. *Yaws' Handbook of the Thermodynamic Properties for Hydrocarbons and Chemicals*. 2009.

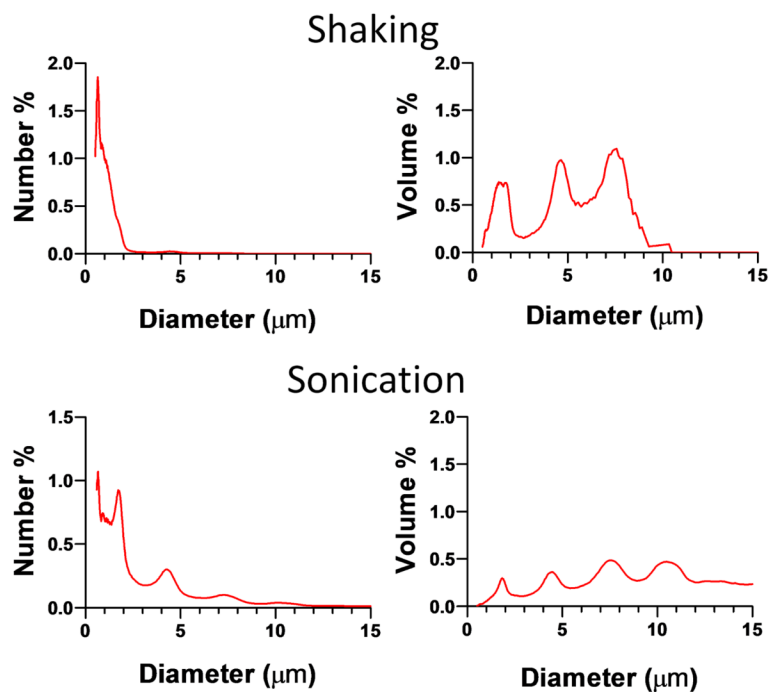


Figure 1. Size distributions of freshly made microbubble suspensions. Microbubbles were formulated using a Vialmix shaker for small volumes of lipid solution (2 mL) and probe sonication for large volumes of lipid solution (120 mL). All lipid solutions (2 mg-lipid/mL) consisted of DSPC and PEG40S at a 9:1 molar ratio.

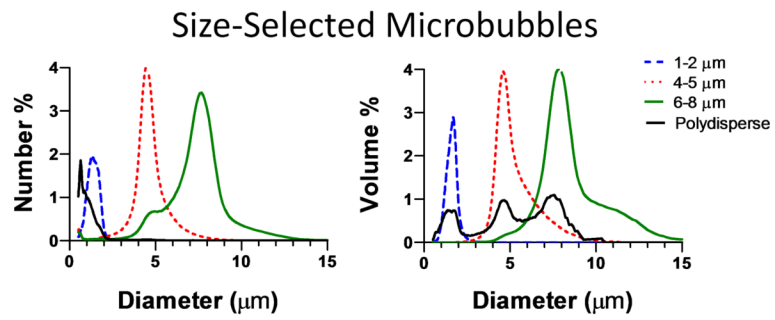


Fig. 2. Size distributions of size-selected microbubbles. The microbubble populations for the individual 1-2 μm (blue), 4-5 μm (red), and 6-8 μm (green), samples are shown as number-weighted and volume-weighted size distributions. The polydisperse sample (grey) is from a freshly made microbubble suspension generated using a shaker.

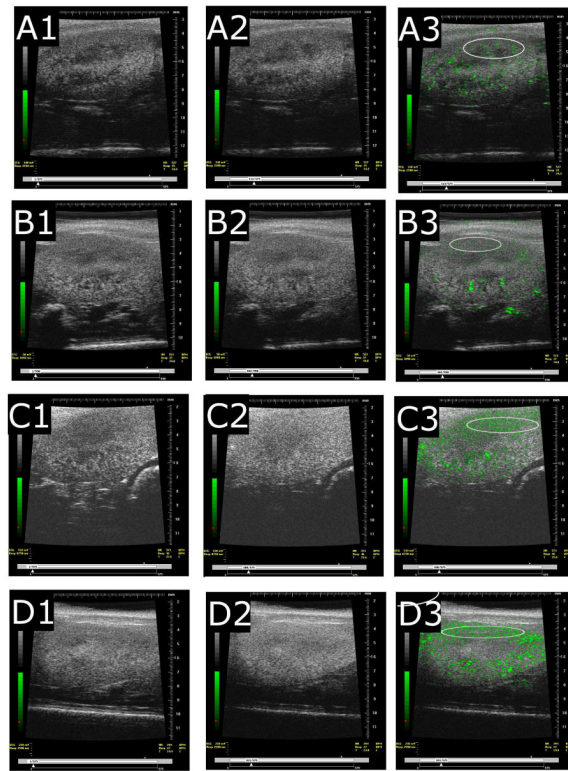


Figure 3.

Contrast enhancement in the kidney following bolus injections of size-selected microbubbles. Microbubble suspensions of 100 μL containing 5×10^7 MB of (A) polydisperse, (B) 1-2 μm , (C) 4-5 μm , or (D) 6-8 μm diameter bubbles were injected intravenously into anesthetized mice while continuously imaging the kidney using a 40-MHz ultrasound probe. Grayscale images are shown before the bolus is injected (A1-D1) and at the peak signal intensity (A2-D2), typically 30-60 seconds after the bolus was delivered. Contrast detection software was used to highlight the presence of microbubbles in green (A3-D3). Areas outlined in white are ROIs selected for TIC analysis.

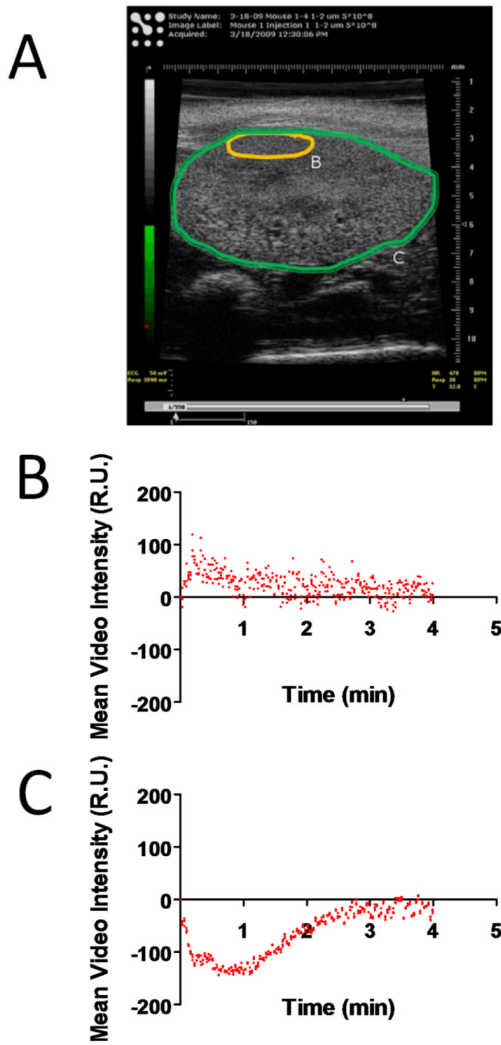


Figure 4. Attenuation of the ultrasound signal from 1-2 μm bubbles. (A) The change in video intensity caused by the 1-2 μm bubbles was evaluated over two regions of interest. Typically, a smaller region of interest in the upper portion of the kidney (yellow) was used to avoid effects of attenuation and shadowing. The larger region of interest (green) encompassed areas deeper within the tissue, which were prone to shadowing and attenuation by microbubbles. (B) The relative acoustic backscatter of the ultrasound signal from the 1-2 μm bubbles showed little signal enhancement above noise in the smaller region of interest. (C) The 1-2 μm bubbles showed strong attenuation of the signal, as determined by whole kidney as the region of interest.

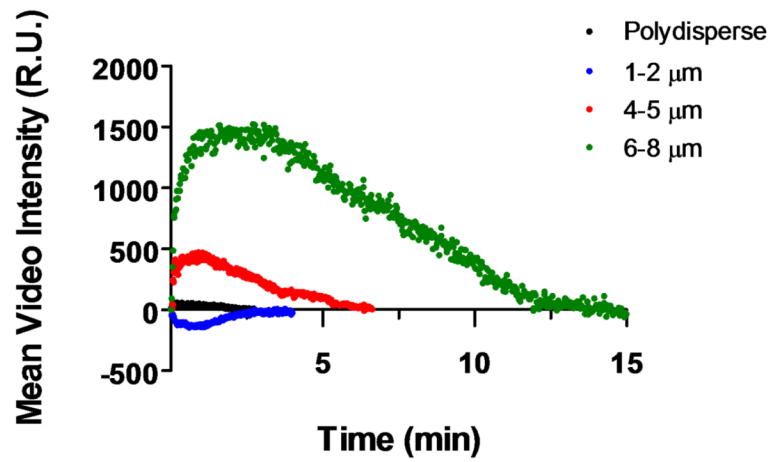


Figure 5. Time-intensity curves in the mouse kidney following bolus injections of size-selected microbubble suspensions. Representative TIC's are shown for each size-selected population after a 100 μ L bolus injection of 5×10^7 MB. All data was offset corrected using background images as a reference.

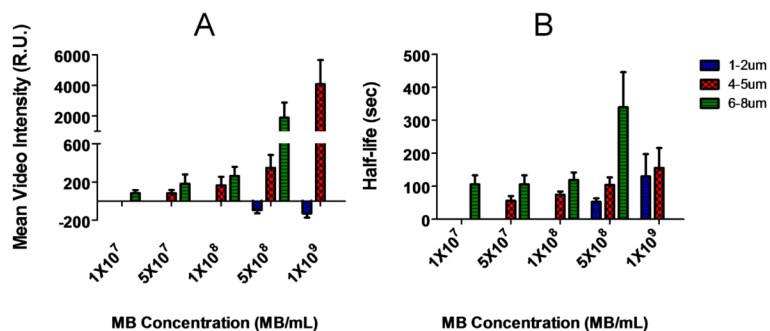


Figure 6. Signal amplitude and half-life of size-selected microbubbles. The signal amplitude and total contrast persistence was measured from the TIC's over a range of microbubble concentrations. (A) The signal amplitude was determined by the maximum signal intensity from the TIC for each microbubble sample. For 1-2 µm bubbles which attenuated the signal, the minimum signal intensity value was used. (B) The half-life of the signal was determined from the TIC at the time the signal intensity decayed to half of the maximum amplitude.

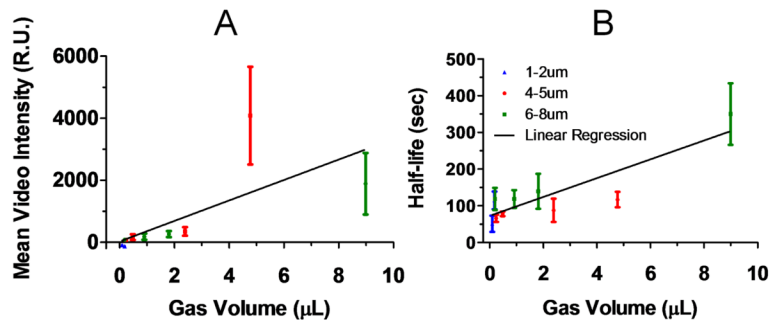


Figure 7. Signal amplitude and half-life of size-selected microbubbles as a function of total gas volume. The signal amplitude values (A) and half-life values (B) are the same as shown in Figure 6.

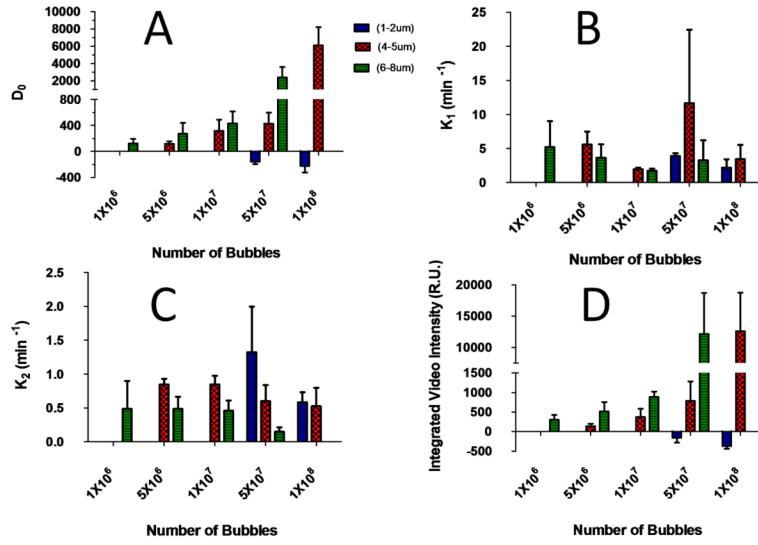


Figure 8. Parameters for model fit of TIC. Each TIC was fit to a model describing the influx and decay of contrast agent in the kidney (equation 1 in Appendix). The parameters were determined by fitting the data to the equation using least squares regression analysis. (A) D_0 is proportional to the signal intensity. (B) k_1 is a measure of the influx rate of the contrast agent into the kidney. (C) k_2 is a measure of the decay rate of the ultrasound contrast signal. (D) AUC is a measure of the total integrated contrast enhancement determined by the area under the fitted curve.

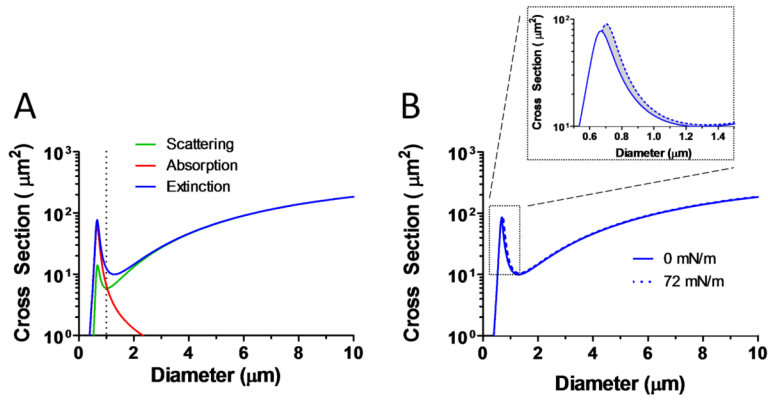


Figure 9. (A) Extinction cross-section as a function of diameter. The extinction cross section, absorption cross section and scattering cross section were calculated using equations derived by Medwin (Medwin 1977) with an additional damping coefficient due to frictional loss (de Jong et al. 1992; de Jong and Hoff 1993) (B) The effect of surface tension on extinction cross-section. The extinction-cross-section as a function of diameter was plotted for low (0 mN/m) and high (72 mN/m) surface tensions to determine the effect of rapidly changing surface tension on the microbubble shell in an ultrasound field. Grey area represents surface tensions between 0 and 72 mN/m.